# Visualization Study on the Flowfield of Rotating Detonation

Wei Lin, Jin Zhou*, Shijie Liu, Zhiyong Lin
Science and Technology on Scramjet Laboratory, National University of Defense Technology
Changsha, 410073, China

## 1 Introduction

The feasibility of continuously rotating detonation and propulsive concept of utilizing rotating detonation were first studied by Voitsekhovskii [1] and Nicholls [2], respectively. Concentrated in the past decade continuously rotating detonation has been extensively studied both experimentally and numerically because of its theoretically higher thermodynamic efficiency than constant pressure combustion and other advantages [3]. People hope to develop a rocket based, air-breathing based or combined-cycle rotating detonation engine (RDE), whose performance could be abreast of or superior to current chemical propulsion [4].

Experimentally, Bykovskii and Zhdan et al. extensively explored continuously rotating detonation phenomena [5], their studies involve various explosive mixtures, basic flow structure and required chamber length. Wolański [4] and Kindracki [6] et al. successfully achieved initiation of rotating detonation in different fuel/oxygen mixtures and hydrogen/air mixture. They established the range of propagation stability as a function of the chamber pressure, composition, and engine geometry. Eric M. Braun et al. tested several fuel/oxygen mixtures in swirled-flow injection mode and analyzed the rotating detonation propagation [7]. Liu and Lin et al. [8,9] experimentally summarized the existing range and the propagation mode of rotating detonation in hydrogen/air. Moreover, 2 D and 3 D simulations in continuously rotating detonations have been carried out. Some key issues, including the fuel injection limit [10], self-ignition, thermodynamic performance have been discussed. Some fine structures of the rotating detonation have been simulated to help understand the flowfield of the rotating detonation. [11]. Typically, The effects of various configurations of the RDE on the flowfield and the propulsive possibility have been numerically studied[12]. Additional, the thrusts of the rocket-based RDE model engines were also measured while detonating hydrogen/air by James A. Suchock et al [13], hydrogen/oxygen by and methane/oxygen by Wolański et al. [4]. kerosene/oxygen by Bykovskii et al. [5].

In spite of the mentioned contributions, basic flowfield structure of rotating detonation and its propagation mechanism has yet to be fully interpreted. Some technical methods are confined by the annular shape, such as schlieren photography and other laser diagnostic techniques (e.g., PLIF) are difficult to be utilized. Consequently, visualized experimental results on rotating detonation flowfield structure are scarce. Moreover, the simulation results are hard to cover all the real physics of a detonation, e.g., pre-ignition and involving a real injection process. In present study we presented the experimental physics of the rotating detonation wave in two mixtures of $H_2$/air and $CH_4$/$O_2$. Distinct momentary photographs were illustrated for understanding the flowfield structure.

*Correspondence to: zj706@vip.sina.com 

## 2 Experimental setup

A schematic of the test configuration is illustrated in Figure 1. Corresponding physical model is designed without specific cooling and made with stainless steel. It has an annular combustion chamber with a sleeve diameter of 100 mm and a sleeve length of 75mm measured from an oxidizer injection nozzle. The thickness of the annular chamber δ is 5 mm. The oxidizer is injected axially from this annular Laval nozzle slit with a 0.4 mm wide throat encircling the fuel injection manifold. The fuel is injected through 90 sets of injection orifices with a 0.8 mm diameter. These injection orifices have a 60 degree incidence angle measured from axial line and are evenly distributed surrounding the inner core. A quartz glass window is equipped for observation (50 mm in longitudinal direction × 30 mm in circumferential direction, its inner side has the same curvature as the sleeve), upper end of this glass window locates 5 mm downstream from the oxidizer nozzle throat. In order to measure the pressures in the combustor, seven pressure taps are set along the axis of the outer sleeve wall. These taps have a pitch of 10 mm and are located 5mm downstream of the oxidizer throat. PCB high-frequency dynamic piezoelectric transducers are mounted on the sleeve wall along the axial direction.

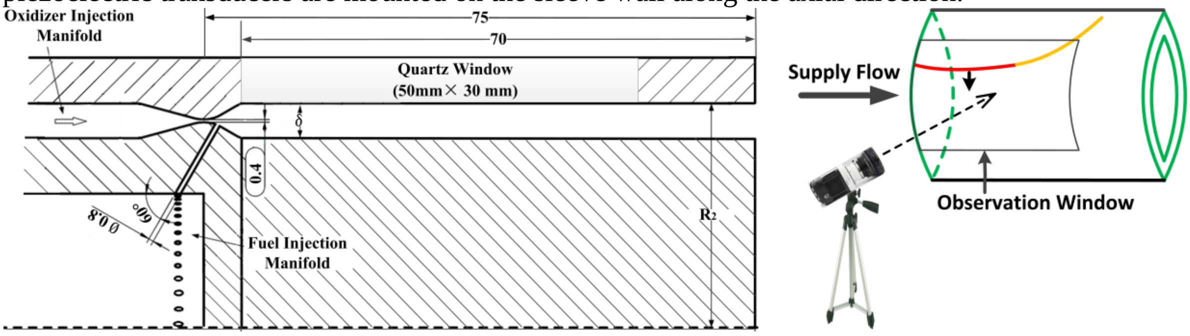


Figure 1. Rig of the experimental setup. Left: A schematic of the test configuration. Right: Visualization setup

The propellant delivery system is designed to supply a required stable gas flow for detonation combustion test, with several high-pressure propellant source tanks of air, $O_2$, $N_2$, $CH_4$ and $H_2$. High-pressure gaseous sources are controlled and regulated by electromagnetic valves, pressure reducing valves, one-way check valves, filter valves and pressure safety valves. Consequently the equivalence ratio of the propellants can be adjusted within a wide range.

Experiments were conducted and strictly followed specific preset time sequences shown in [9]. A pre-detonation tube fed with $H_2/O_2$ is used to ignite the model. The measure and control system is applied to control the experimental process and acquire experimental signals. These signals include the high frequency pressures of detonation waves captured by PCB 113B24 piezoelectric transducers, and the pressures in injection manifolds and combustion chamber measured via the injection pressure taps on the manifolds and six pores along the axis of the outer sleeve wall, respectively. A high-speed camera FASTCAM SA5 was employed for the purpose of intuitively observing the flow field structure of a detonation. In this paper, an imaging velocity of 150,000 fps was put to use. The camera was horizontally lain on a tripod and perpendicularly focused on the center of the side window, the distance was about 1 m away (the distance depends on the focal length), and the center of the lens and the window horizontal level stayed at the same height (refer to Figure 1).

## 3 Result and discussions

Table 1: Supply conditions and working parameters of the detonation process

| Cases | Mixture | $P_f$, $MPa$ | $P_o$, $MPa$ | $\dot{m}_f$, g s$^{-1}$ | $\dot{m}_o$, g s$^{-1}$ | $\dot{m}$, g s$^{-1}$ | $\dot{m}/A$, kg s$^{-1}$ m$^{-2}$ | $\phi$ | $D$, $m\ s^{-1}$ | $f$, $kHz$ | $n$ |
|---|---|---|---|---|---|---|---|---|---|---|---|
| 1 | $H_2$/air | 0.526 | 0.978 | 12.5 | 490.2 | 502.6 | 177.79 | 0.878 | 1688 | 5.97 | 1 |
| 2 | $CH_4/O_2$ | 1.07 | 0.617 | 58.6 | 224.6 | 283.2 | 189.78 | 1.046 | 2213 | 14.83 | 2 |

Table 1 presents the supply conditions and the working parameters of the detonation process for cases these two cases, detonating $H_2$/air and $CH_4/O_2$ respectively.

## 3.1 $H_2$/air detonation propagation analysis

In case # 1, the injection pressures for $H_2$ and air were 0.526 Mpa and 0.978 Mpa respectively. $H_2$ was supplied at a mass flow rate of 12.5 g $s^{-1}$, air was supplied a mass flow rate of 490.2 g $s^{-1}$. The total mass flow rate was 502.6 g $s^{-1}$, with a corresponding equivalence ratios $\phi$ 0.878 (lean fuel).

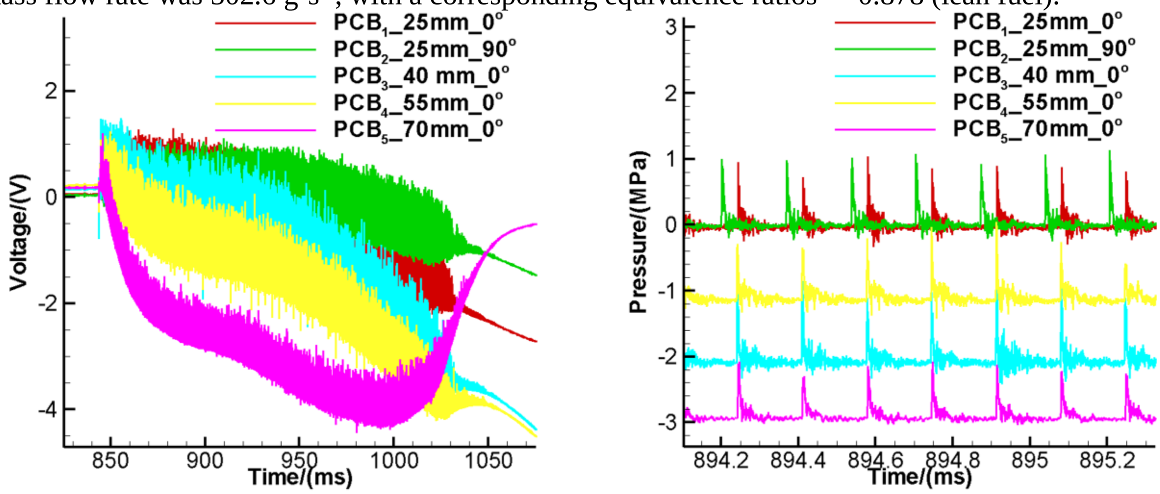


(a) (b)

Figure 2. History of high frequency pressure. Left: The original signal for the pressure history shown in Voltage. Right: The magnified pressure oscillations

Figure 2 shows the history of high frequency pressure for case #1. 5 PCB transducers were mounted at different places to record the pressure oscillations. $PCB_1$_25mm_0°, $PCB_1$_40mm_0° $PCB_1$_55mm_0°, $PCB_1$_70mm_0° were placed along the same longitude, the postfix distances present the distance downstream of the oxidant injection throat. While $PCB_2$_25mm_90° was placed 90° anticlockwise ahead if viewing from the inlet direction. After some transforms and operation of magnification, the specific pressure oscillations are displayed, from which the height of the detonation could be approximately estimated to be within 25 - 40mm. Because the phasic difference between $PCB_1$_25mm_0°, $PCB_1$_40mm_0° is significantly exceeds those between the others, e.g., $PCB_1$_40mm_0° $PCB_1$_55mm_0°.

Measuring the interval of each two ordinal waves, an instantaneous average frequency in one cycle could be computed. Counting all the N cycles, an average frequency of rotating detonation waves could be obtained. By this method, an average frequency of 5.97 kHz is derived. The rotating detonation detonating $H_2$/air mixture propagated in an average velocity of 1688 m/s with single head.

Three sequential frames of luminous reaction zones of a rotating detoantion wave are gathered in Figure 3. Note that the rotating detoantion wave propagated from left to right across the window region. Because $H_2$/air combusiton doesn't release amply bright light. The frames has been enhenced in the luminance. At t=0 μs, the detonation wave (frame A) just entered the observation window. 6.67 μs later, a luminously zone (frame B) was captured, whose upper bright edge zone represented the reaction zone of the $H_2$/air detoantion wave. At t=13.33 μs, an entire rotating detoantion wave (frame C) was visible. Combined the window width 30 mm and the 150,000 fps imaging speed, approximately momentary detonation velocity was computed to be 1700 -1750 m $s^{-1}$. This velocity approaches the average velocity computed from the pressure oscillations above. These frames not only provide an intuitive description of the rotating detonation and the instantaneous propagating velocity, but are efficient means to estimate the structure of CRDWs. (e.g., height of the reaction zone, oblique shock wave and its deflection). Estimate from the rough luminous zone height, the detoantion wave should be maintained within a height of within 25 mm.

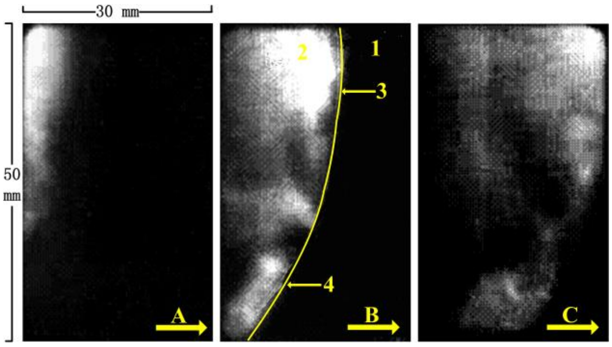


Figure 3. Sequentially high-speed optical observation of rotating detonations passing across the observation window: frame A, 0 μs; frame B, 6.67 μs; frame C, 13.33 μs

A rough sketch of the detonation wave could be identified from the sharp interface. For example, as shown in frame B, "1" denotes the fresh mixture layer zone, "2" indicates the combusted gas zone, "3" points to the interface of the dark and bright zones, and its left interface illustrates the boundary that reaction zone begins. "4" presents the oblique shock wave structure caused while detonated product expands to the outlet. This structure is also in agreement with the typical simulation structure.

## 3.2 $CH_4/O_2$ detonation propagation analysis

In case #2, the injection pressures for $CH_4$ and $O_2$ were 1.07 Mpa and 0.617 Mpa respectively. $CH_4$ was supplied at a mass flow rate of 58.6 g $s^{-1}$, $O_2$ was supplied a mass flow rate of 224.6 g $s^{-1}$. The total mass flow rate was 283.2 g $s^{-1}$, with a corresponding equivalence ratios $\phi$ 1.046.

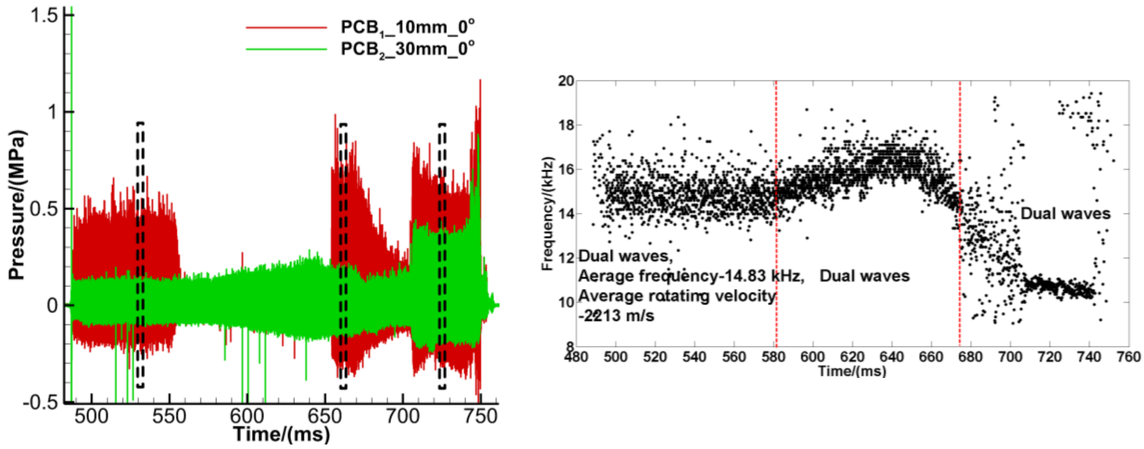


Figure 4. History of the high frequency pressures

The history of high frequency pressures of case # 2 and the freqnency distribution in time-domain are presented in Figure 4. $CH_4/O_2$ CRDWs propagated in stable dual wave mode with an average frequency of 14.83 kHz and an average velocity of 2213.4 m $s^{-1}$. Starting from 593 ms, $N_2$ and air entered the injection manifolds, therefore pressure waveform in Figure 4(a) presents a gradual increase of the amplitude due to a greater mass flow rate. However, the frequency from 582 ms to 678 ms shows a first increase and then decrease tendency as the total mass flow rate was increasing but the sensitivity was decreasing. The frequency-time relationship in Figure 4(b) indicates CRDWs in unstable $CH_4/O_2/N_2$ mixture were maintained in dual wave mode. From 703 ms to 743 ms, since air and $N_2$ have reached a relative normal supply, waveform of $CH_4/O_2/N_2$ detonation was much higher and uniform even more air and $N_2$ were injected, detonation waves still propagated in dual wave mode but shifted to lower velocity in the equivalent $CH_4/O_2/N_2$ mixture (consider mole ratio of $O_2$ and $N_2$ in air to be 1:3.76) with an approximate mole ratio 1:2.28:2.52. Corresponding to the above analysis, enlarged waveforms in stable $CH_4/O_2$ phase, unstable $CH_4/O_2/N_2$ phase and stable $CH_4/O_2/N_2$ phase are abstracted in Figure 5(a), Figure 5(b) and Figure 5(c).

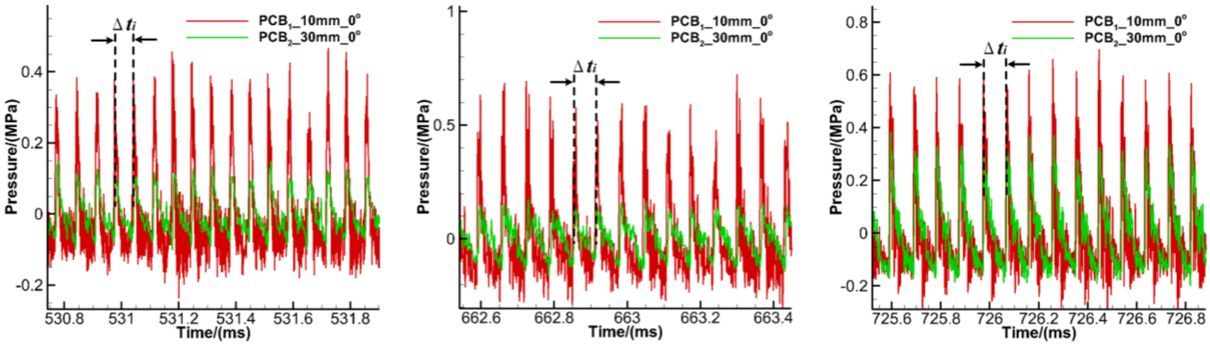


(a) (b) (c)

Figure 5. (a) Enlarged PCB high frequency pressure at $CH_4/O_2$ phase; (b) Enlarged PCB high frequency pressure at unstable $CH_4/O_2/N_2$ phase; (c) Enlarged PCB high frequency pressure at stable $CH_4/O_2/N_2$ phase

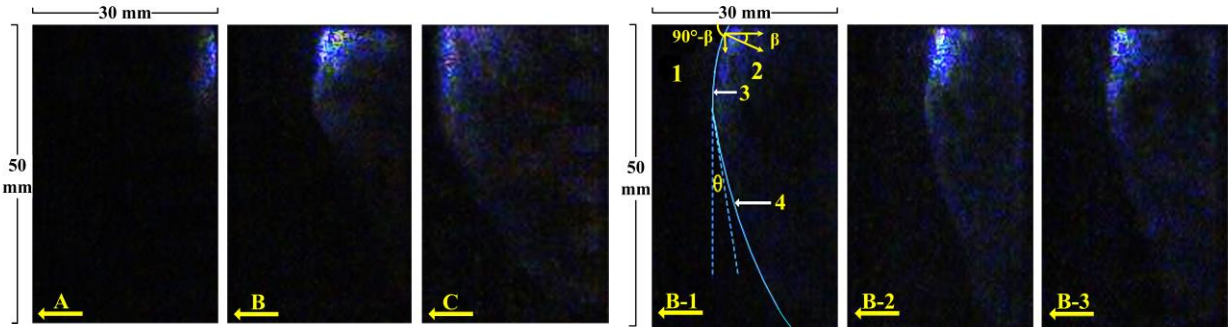


(a) (b)

Figure 6. Sequentially high-speed optical observation of CRDWs passing across the observation window: (a) Sequential 3 frames (frame A, 0 µs; frame B, 6.67 µs; frame C, 13.33 µs); (b) 3 frames in sequential 3 circles (frame B-1, 0 µs; frame B-2, 6.67 µs; frame B-3, 13.33 µs)

Luminous light intensity usually will be observed in detonation of gaseous hydrocarbon mixture, which therefore shows a good observability for identifying specific detonation structure. The entire process (i.e., ignition by $H_2/O_2$ detonation jet, $CH_4/O_2$ detonation phase and $CH_4/O_2/N_2$ detonation phase) was photographed through longitudinal windows in the combustor by a high-speed camera. And several frames of $CH_4/O_2$ detonation phase were listed below.

Combined the window width 30 mm and the 150,000 fps imaging speed, approximately momentary detonation velocity was computed to be 2000 - 2200 m $s^{-1}$. A rough sketch of the detonation wave could also be identified from the sharp interface.

It is interesting to identify the rough height of the detonation wave and the dragging angle of the oblique shock wave. The former is ~16-20 mm and the latter has a vertical deflection θ approximately 10.5°. Furthermore, the high-speed optical photographs show the marginal expansion area of the oblique shock despite oblique shock itself is not luminous. Transient structures of frames B-1, B-2 and B-3 in Figure 6(b) present subtle differences, which is related to the instability of the detonation itself and the viewing angle.

Frame B-1 in Figure 6(b) also presents a inclined tendency. Define the angle between the inclined detonation wave and the vertical axis line as β, then the angle between the detonation wave and top end is 90°-β. We fix the detonation wave, thus a detonation velocity triangle relationship is established on the detonation wave. Note that the circumferentially partial velocity is the inverse propagation velocity of the detonation wave, the axial partial velocity corresponds to the propellant injection velocity, and the resultant velocity which is perpendicular to the inclined detonation front is the detonation velocity. Based on this, since we measure the β to be ~10°in frame B-1and have known the average propagation (rotating) velocity $\overline{V}$ (2253.3 m $s^{-1}$). Thus, the injection velocity could be estimated by the relationship $V_{jet} = \overline{V} * \tan\beta$, it is ~400 m $s^{-1}$. And the resultant velocity of detonation wavefront is derived from the relationship $V_{jet} = \overline{V} / \cos\beta$, it is 2288 m $s^{-1}$. However, a velocity deviation of injection entrance velocity for fresh gaseous mixture is inevitable, because it is the fresh gaseous mixture has a velocity gradient in vertical direction, moreover, propellants are injected separately.

# 4 Conclusions

The high-speed photography provides an excellent method to help to explain the propagation and detail structures of continuously rotating detonation waves in mixtures of $H_2$/air and $CH_4/O_2$. Therefore from the frames, momentary velocity and specific structure, such as approximately height of detonation wave, oblique shock wave and its deflection angle, and even the injection velocity could be estimated.


# Acknowledgements

This work is supported by the National Natural Science Foundation of China, Grant Nos. 51306202 and 51476186.


# References


[1] Voitsekhovskii BV. (1959). Maintained detonations. Doklady Akademii Nauk UzSSR. 129: 1254.

[2] Nicholls JA. (1964). The feasiblility of a rotating detonation wave eocket motor. Technical documentary report. No. PRL-RDR-64-113.

[3] Zhou R, Wang JP. (2012). Numerical investigation of flow particle paths and thermodynamic performance of continuously rotating detonation engines. Combust Flame. 159: 3632.

[4] Wolanski P. Detonative propulsion.(2013). P Combust Inst. 34: 125.

[5] Bykovskii FA, Zhdan SA, Vedernikov EF. (2013). Reactive thrust generated by continuous Detonation in the air ejection mode. Combust Explo Shock+. 49: 188.

[6] Kindracki J, Wolański P, Gut Z. (2011). Experimental research on the rotating detonation in gaseous fuels–oxygen mixtures. Shock Waves. 21: 75.

[7] Braun EM, Dunn NL., Lu FK. Testing of a continuous detonation wave engine with swirled injection. AIAA 2010-146.

[8] Liu SJ, Lin ZY, Liu WD, Zhuang FC. (2012). Experimental realization of H2/Air continuous rotating detonation in a cylindrical combustor. Combust Sci Technol. 184: 1302.

[9] Lin W, Lin ZY, Liu SJ, Zhuang FC. (2015). Experimental study on propagation mode of H2/Air continuously rotating detonation wave. International Journal of Hydrogen Energy Hydrogen. Online published.

[10] Wang J P, Shao S T. Rotating detonation engine injection velocity limit and nozzle effects on its propulsion performance. Computational Fluid Dynamics 2010. 2011; 789-795.

[11] Hishida M, Fujiwara T, Wolanski P. (2009). Fundamentals of rotating detonations. Shock Waves. 19: 1.

[12] Schwer DA, Kailasanath K. Numerical study of the effects of engine size on rotating detonation engines. AIAA 2011-581.

[13] Suchocki JA, Yu STJ, Hoke JL, Naples AG, et al.. Rotating detonation engine operation. AIAA 2012-0119.